New Ways of Looking at Masks with the SHARP EUV Microscope

Kenneth A. Goldberg,* Markus P. Benk, Antoine Wojdyla, David G. Johnson,
and Alexander P. Donoghue
Lawrence Berkeley National Laboratory, 1 Cyclotron Rd., Berkeley, CA USA 94720

ABSTRACT

Extreme ultraviolet (EUV) microscopy is invaluable for the development of EUV photomasks, providing detailed information for the creation of new mask processes, and reliable feedback for comparison with printing studies. The SHARP microscope at Lawrence Berkeley National Laboratory is dedicated to photomask research. It was developed with forward-looking specifications that make it well suited to the emulation of current EUV lithography tools and a variety of possible future directions. Some recent examples include (1) the demonstration of imaging with 4x numerical aperture values up to 0.625, measuring patterns with feature sizes down to 30-nm half-pitch, created with a tin-based photoresist serving as the absorber. (2) The emulation of complex, free-form illuminators used in source-mask optimization, including grayscale pupil fills. (3) Point by point phase measurement from aerial image measurements using several techniques. (4) Direct observation of non-telecentric, through-focus imaging effects that arise from the angular-dependence of the mask's multilayer coating properties. In addition, we are preparing to extend SHARP imaging to include anamorphic optics, an emerging area of EUV lithography research.

Keywords: EUV, mask, microscope, actinic, illumination, phase, resolution, zone plate

1. INTRODUCTION

SHARP is an extreme ultraviolet (EUV), *actinic* microscope dedicated to photomask research. The design and operation of SHARP have been described in several previous publications.[1–4] Briefly, SHARP is based on a synchrotron bending-magnet beamline that delivers narrow band EUV light with a small angular divergence. SHARP's Fourier-synthesis illuminator[5] uses a MEMS-based, angle-scanning, multilayer-coated mirror and an elliptical condenser to create arbitrary angular pupil fill patterns up to 19° off-axis at the mask. A Fresnel zoneplate lens, fabricated with electron-beam lithography in patterned gold on a silicon-nitride membrane, captures the reflected light and projects a high-magnification image with diffraction-limited quality onto an EUV-sensitive charge-coupled device (CCD) camera. Hundreds of user-selectable zoneplates are installed in SHARP: they have various optical properties with low and high-numerical aperture designs, and some include wavefront-engineering for advanced microscopy modes.[6–8] SHARP's mask stage allows measurements to be performed across the entire mask surface, on blank or patterned masks, with a coordinate systems based on local mask fiducial features.

SHARP is used in nearly every aspect of EUV photomask research, including programmed and native defects,[9–11] repair stratgies,[9,12,13] mask materials and architecture,[12] mask surface and absorber-pattern roughness,[14] optical proximity correction (OPC) and assist features,[15] phase-shifting masks, and the investigation of various illumination conditions and coherence states.[16]

To date, most of the work with SHARP is concentrated in these areas using optical conditions that emulate current and planned EUV projection lithography tools, with 4x numerical aperture values of 0.25 and 0.33. Recent advances have demonstrated SHARP's forward-looking capabilities. Advances in spatial resolution, phase measurement, illumination, image-properties, and new lens designs are discussed in the context of recent advances in our field.

2. SCALING FOR FUTURE NODES

SHARP is capable of scaling to significantly smaller mask pattern dimensions than are currently used. We recently created two resolution tests masks to evaluate the performance and performance limits of SHARP. The first mask is a conventional patterned reticle we refer to as the *Calibration Test Mask*. It was designed to support resolution testing and it will be measured repeatedly, over time, to assess the performance and self-consistency of SHARP's imaging. The second mask was an experimental *Wafer Test Mask*, with patterning below 30 nm half-pitch.

*KAGoldberg@lbl.gov; phone 1 510 495-2261; fax 1 510 486-4550; sharp.lbl.gov

Extreme Ultraviolet (EUV) Lithography VI, edited by Obert R. Wood II, Eric M. Panning,
Proc. of SPIE Vol. 9422, 94221A · © 2015 SPIE · CCC code: 0277-786X/15/$18
doi: 10.1117/12.2175553

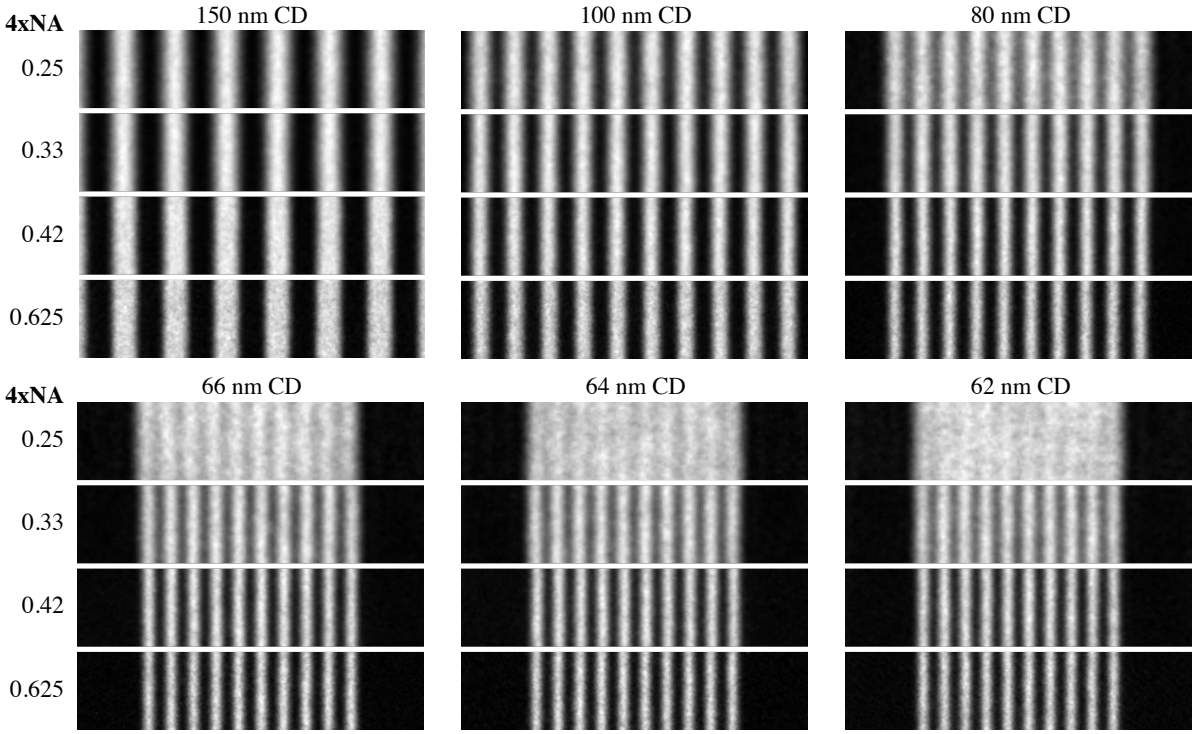

Figure 1. Vertical 1:1 lines imaged in SHARP with four different NA values. Each detail is 2.0-µm wide. The partial coherence σ value was 0.8, adjusted to the NA, for each measurement. The contrast reduction observed in features imaged with the lower-NA lenses shows the resolution limit of those lenses.

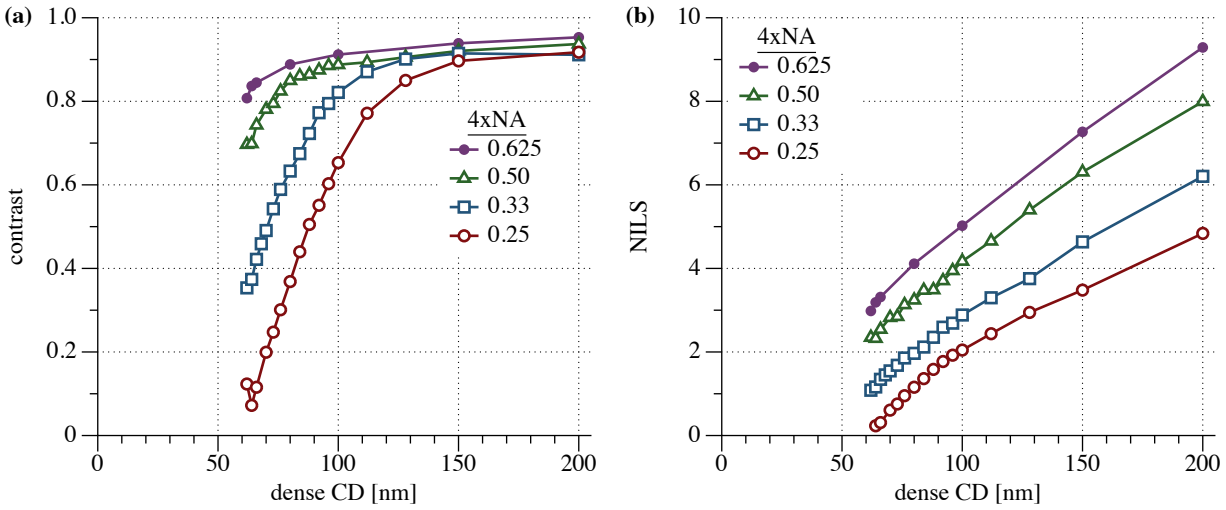

Figure 2. Measured, best-focus **(a)** contrast and **(b)** NILS versus CD for dense vertical lines and four different NA values, and partial-coherence σ of 0.8. Each data point represents a separate through-focus series and therefore an independent measurement of these imaging parameters. As expected, the higher-NA lenses in SHARP offer significantly improved resolution and higher image log slope.

2.1 Calibration Test Mask

The Calibration Test Mask was made by *Intel* with resolution test structures that include 1:1 dense lines in the vertical and horizontal directions. SHARP imaged these lines through-focus using several different lens NA values. A partial-

coherence σ value of 0.8 (scaled to the lens NA) was used for all of the measurements. Images are shown in Fig. 1 for several line sizes. At and below 60-nm half-pitch (mask scale), the lines suffered from pattern collapse and were not imaged.

Contrast and NILS were extracted from the best-focus images in each series, using an intensity threshold level that produced line widths matching the half-pitch. Figure 2 contains the measured contrast and NILS curves. The observed contrast and image slope arise from a combination of the mask and lens properties, and the illumination coherence state. Based on partially coherent measurements of the 200-nm CD lines, using the 0.33 and 0.625 4xNA lenses we found that the maximum image contrast is 93.6 and 95.3%, respectively, on this mask.

2.2 EUV-printed wafer test mask

Our goal with the Wafer Test Mask was to overcome the fabrication limits of conventional EUV mask patterning by using patterns printed with EUV lithography, in photoresist, on a silicon wafer. The mask was created on a 6-inch silicon wafer with a conventional Mo/Si EUV multilayer, coated with resist, and exposed in the Berkeley Microfield Exposure Tool (BMET).[17] Printing directly into photoresist and developing in a single step simplified the mask-creation process by eliminating the need to subsequently etch into an absorber. An experimental tin-based photoresist from *Inpria* was selected for its high absorption relative to organic, chemically amplified photoresists.[18] The one mask sample that was created had a photoresist layer of approximately 12 nm, which is lower than expected. This leads to a reduced overall contrast (12% peak) and pattern quality. Nonetheless, the modulation apparent in the images of small features (see Fig. 3) is enough to demonstrate the high-resolution performance of SHARP. The images shown are among the smallest lines we have observed in SHARP to date.

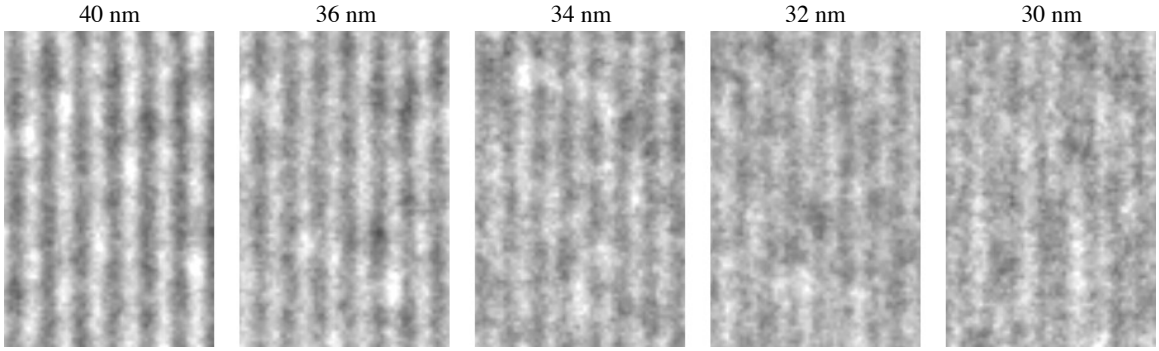

Figure 3. EUV images of dense vertical lines from the Wafer Test Mask recorded with SHARP's 0.625 4xNA lens, and 0.85 σ. Test patterns were created in a tin-based *Inpria* photoresist, printed with the BMET. The resist layer is thinner than expected, and the peak contrast is close to 12% for large features. Modulation at 30-nm half-pitch is visible. Note that the image contrast has been individually scaled for visualization.

3. TESTING FUTURE SOURCE CONFIGURATIONS

Progress in photolithography relies on highly engineered illumination coherence states. The angular distribution of the illumination can be tuned to affect the resolution, image slope, edge placement, and through-focus properties.

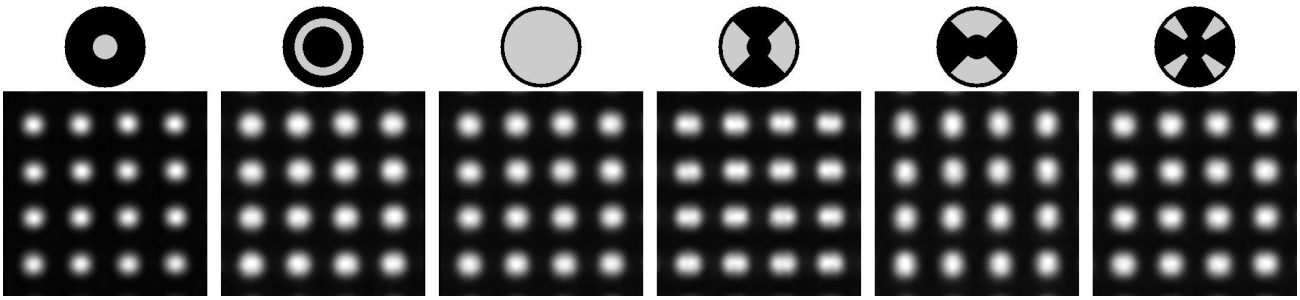

Figure 4. Dense, square, 175-nm-wide (mask scale) contacts imaged with SHARP's 0.33 4xNA lens and various illumination conditions. The images are 1.5-μm on edge, and the pupil-fill patterns are represented above the images.

SHARP's scanning illuminator can emulate a wide variety of current or future source configurations. The demonstration and use of "conventional" pupil-fill patterns has been well established.[4] Disk, annular, dipole, cross-pole, Quasar, and other patterns are commonly requested by SHARP's users. Figure 4 shows a dense array of square contacts imaged with various illumination settings selected to demonstrate the strong coupling between illumination and image formation.

At its most coherent setting, SHARP's illumination is approximately 0.05 σ at 0.25 4xNA: the full-angle is close to 6-mrad divergence. All other pupil fills are created by scanning the narrow, coherent beam through an angular pattern. Scans are typically cycled more than ten times within each 5–8 second exposure. The scan speed is fast enough that the amount of unblocked light entering the dark regions between the isolated bright areas is insignificant.

We measure the illumination pattern in SHARP directly, using an upward-facing, in-vacuum microscope with a YAG-crystal scintillator.[3] The YAG can be placed in or below the illuminator's focal plane to assess the central ray angle and angular spectrum of the illumination.

3.1 Demonstration of free-form source profiles

Modern lithographic printing tools now incorporate a high degree of source customization through the use of faceted or pixelated, *free-form* sources.[19,20] Such illuminators enable researchers to computationally optimize pupil fills to maximize the process window for printing given features. This area of research is referred to as *source-mask optimization* (SMO).[21–23] Free-form pupils typically contain a two-dimensional set of fixed angular components that can be switched *on* or *off* to deliver light from specific angles, making what is effectively a discrete, binary, angular spectrum.

SHARP's illuminator can be programmed to produce free-form pupil fills, enabling SMO studies to be made using real image data rather than simulations as input.[24] SHARP emulates discrete angular spectra by altering the angular scan pattern to dwell for longer times at specific locations in the pattern—the beam sits at a one angle, and then abruptly jumps to the next. For convenience, we created a software interface that uses a two-dimensional input array to encode beam angle positions only where the *pixels* are bright. Examples recorded with the YAG-crystal microscope are shown in Fig. 5. Note that the beam is on continuously during each exposure; the significance of stray light in the dark regions between the designated positions depends on the scanning speed, the number of discrete positions, and the dwell time at each position.

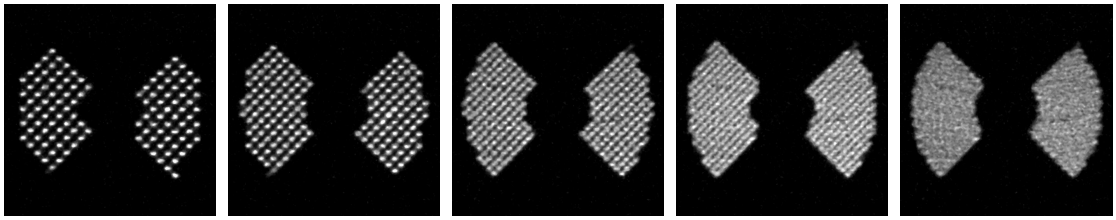

Figure 5. Measured angular pupil fill patterns recorded with an in-vacuum scintillator-based microscope and a 4xNA value of 0.5. The density of the pixelated positions is increased from left to right.

Researchers from *ASML/Brion* have introduced pupil fill patterns with varying degrees of complexity, customized to improve certain imaging metrics.[20,23] With the introduction of the *FlexPupil* illuminator for the *ASML* 33x0 scanners, such patterns are becoming available[19]—SHARP can reproduce them for direct imaging studies and side-by-side comparisons of different illumination conditions. Examples are shown in Fig. 6.

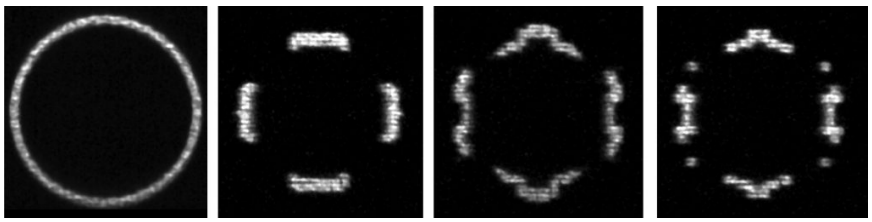

Figure 6. Measured SHARP Pupil fill patterns with 0.5 4xNA, replicating patterns recommended in Ref. 20. The left-most pattern is a simple annulus with σ = 1.0 provided as a reference for the angular range.

3.2 Linearizing the source

Regarding the use and study of complex, discrete source patterns, it is important to understand how each illumination element contributes to imaging. Simulations are useful in this regard, but they cannot fully reproduce the complex interactions between real mask and absorber architectures with the various illumination angles. SHARP can direct individual illumination angles toward the mask, one at a time, allowing us to build up a set of images that can be used for such modeling. Having measured individual images for each illumination direction (or symmetric pairs or quartets of illumination directions at the same time), we can linearize the source description and synthesize arbitrary partially coherent imaging conditions by adding the relevant images in intensity (i.e. as an incoherent sum). This ongoing work was discussed by the authors,[24] and will be the subject of subsequent publications now in preparation.

3.3 Grayscale sources

Ideal pupil fill patterns derived from SMO calculations may have continuous *gray* levels before they are discretized, binarized, or otherwise constrained to match real-world illuminator performance. SHARP's scanning illuminator can go beyond discrete, binary pixelated sources: by modulating the dwell time at each pixel individually, we can create grayscale pupil-fill patterns, such as those shown in Fig. 7. This freedom gives lithographers another lever to optimize pupil fill patterns for specific mask designs. In practice, the number of available gray levels in SHARP depends on the cycle time, the number of non-zero pixels in the illuminator, and the cutoff frequency of the angle-scanning mirror. With fewer pixels and longer image exposure times, a greater number of distinct gray levels can be produced.

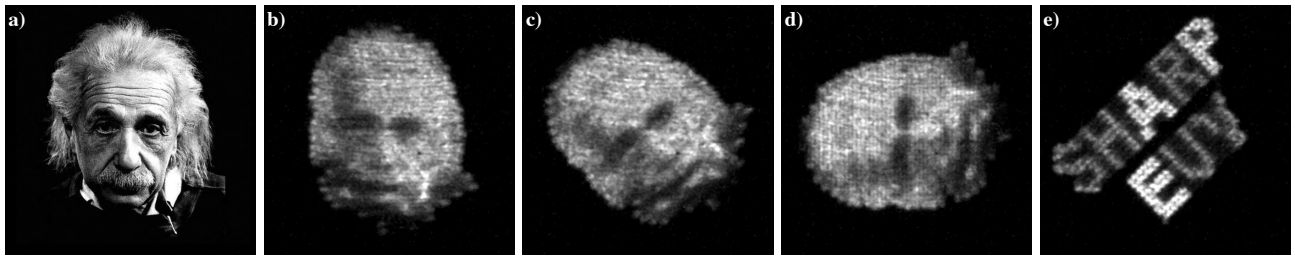

Figure 7. Demonstration of grayscale illumination pupil fills in SHARP. The input image **(a)** was rendered onto a 41x41 pixel grayscale grid and mapped onto angle-space with a 4xNA value of 0.5 **(b-d)**, recorded with the in situ YAG microscope. The letters in image **(e)** were rendered with two different gray levels.

4. IMAGE PHASE MEASUREMENT

When masks are imaged with SHARP, as with most conventional light microscopes, only the intensity is recorded; phase information in the light field is lost. Likewise, photoresists only respond to intensity. However, the importance of phase in image formation should not be discounted. Phase determines how light propagates and is critical for understanding the impact of defects on imaging metrics. We have implemented several ways to determine the phase of the field reflected from the mask surface. This area is a subject of ongoing research; a few of the methods are briefly described below.

4.1 Through-focus phase reconstruction

SHARP records a series of images *through-focus* at each measurement location. Typically, 11 to 21 steps are recorded, with the longitudinal step size set to a fraction of the depth of focus. The most commonly used step size is 400 nm.

We have successfully reconstructed the image phase using a modified Gerchberg-Saxton Method.[25,26] This approach works iteratively to find a complex field in the pupil (i.e. the conjugate plane) that is consistent with all of the images through-focus. Two or more images can be used as input. Under coherent illumination conditions, the known solid angle and sharp cutoff of the lens is used as a constraint in the Fourier-domain; the measured image amplitudes (square root of the intensity) are applied as constraints in the object space. Once the field in the pupil has been solved, the complex amplitude and phase in any image plane can be calculated. In this method, the inclusion of small focal steps is necessary to resolve the sharpest phase gradients; while larger focal separations help to solve lower-spatial-frequency phase information.

4.2 Differential phase contrast

Differential phase contrast (DPC) is an emerging imaging mode that extracts phase information from intensity images recorded with off-axis illumination.[27,28] A series of images is recorded with asymmetric, off-axis illumination patterns and is then combined mathematically to yield a one- or two-dimensional phase gradient. The underlying phase can be solved from one- or multi-directional gradients. An example is shown in Fig. 8.

One interesting and readily apparent aspect of the DPC approach is the enhanced sensitivity to phase bumps that occurs with off-axis illumination. In Fig. 8, the on-axis illumination case (a), the phase bump nearly disappears from view. Yet the off-axis illuminations, (b) and (c), break the symmetry and reveal the defect. A further advantage of DPC is that the data can be collected quickly—no stage motion is required between images, only a re-direction of the illumination.

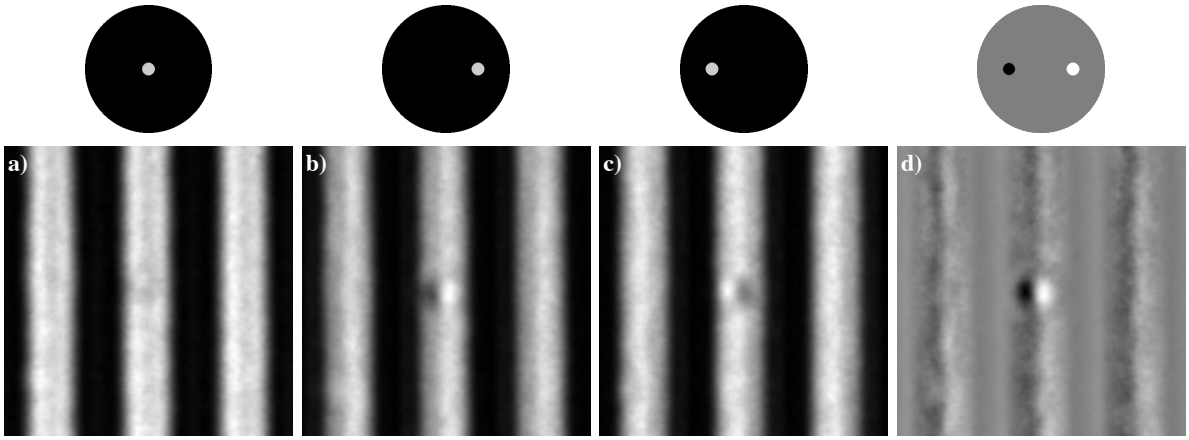

Figure 8. Differential phase contrast measurements of a known phase-defect in the bright area near the center of the 1.5-μm-wide region. The circles above each image represent the angular pupil fill of the illumination. Detail **(a)** is coherent, on-axis illumination. Details **(b)** and **(c)** are off-aixs. Detail **(d)** mathematically subtracts **(c)** from **(b)**, and divides by the average, point by point. The result is related to the phase-gradient in the *x* direction.

4.3 SRAF, effective phase, and Fourier-transform ptychography microscopy

The use of optical proximity correction and sub-resolution assist features (SRAF) are subjects of active research in EUV lithography. As early as 2001, Krautcheck[29] and Yan[30] recognized that the thickness and optical properties of narrow EUV absorber patterns could introduce subtle phase effects in the reflected light field, coming from the index of refraction of the absorber.

Using SHARP, we have observed that effective phase shifts do appear in narrow, SRAF features. Phase changes can be observed indirectly in the Bossung plots of line-features,[30] without sophisticated image processing. When the reflected field has constant phase, and lens aberrations are negligible, we expect imaging properties to be symmetric through focus; in the presence of phase features, asymmetry arises. Figure 9 shows Bossung plots and image slices from two through-focus series: one is a standard line pattern, and the second has a single narrow, interstitial SRAF line.

We are currently developing Fourier ptychographic microscopy (FPM)[31–33] as a new method for extracting both phase and higher resolution from SHARP images. FPM is a computational microscopy method that illuminates the mask sample from different angles and combines the information in the Fourier domain. Overlapping domains build robustness in the phase retrieval. SHARP's illuminator and high static coherence are well suited to the implementation of FPM. Data from FPM, and specifically the analysis of the effective phase in SRAF features, will be presented in a future report, now in preparation.

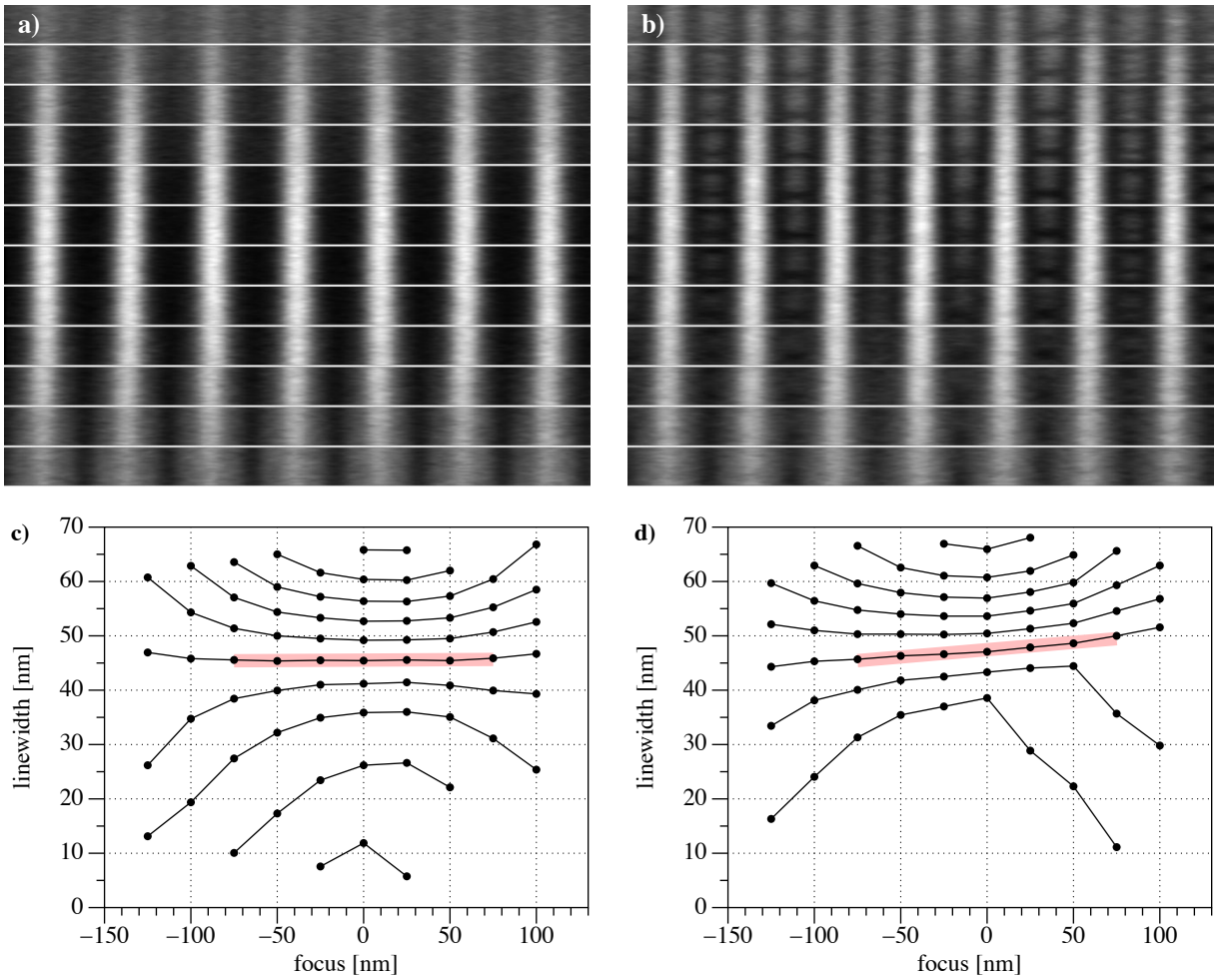

Figure 9. Through-focus image series of lines with 280-nm pitch (mask-scale), analyzed to reveal the line widths at different intensity threshold values, in steps of 10%. **(a,b)** Image details, 2-μm-wide, are shown with the vertical dimension compressed. Each horizontal stripe detail comes from a different image in the series, with 400-nm focal steps between them and the best focus position near the vertical center. The mask patterns shown in **(c)** are comprised of simple lines, while those in **(d)** have a single, narrow SRAF feature between the lines. That feature is more prominent on one side of focus only. In graphs **(c)** and **(d)**, the shaded line highlights the tilt that arises here only in the presence of SRAF features.

5. HIGH-ANGLE MULTILAYER EFFECTS

It is well known that multilayer mirror coatings are *resonant reflectors*, highly sensitive to wavelength, angle of incidence, the *d*-spacing of the coating, and the polarization of the incident light. As such, conventional multilayer coatings used in EUV photomasks have a limited angular bandpass. They reflect efficiently at 6° off-axis, the central ray angle of current EUV optical systems, yet the reflectivity diminishes strongly above 10° or 11°. Various multilayer design strategies can boost the off-axis performance, but gains come at the expense of overall reflectivity, or reflectivity near normal incidence.[34,35]

These angle limitations constrain the usable mask-side numerical aperture to the solid angle that falls within the high reflectivity range. Recent research has predicted that the reflectivity and reflected *phase* difference across the pupil will affect the imaging performance and telecentricity of horizontal lines more than vertical lines at higher NA values.[34–36] Here, *telecentricity* refers to all features in the image having stable relative positions through focus.

SHARP was recently used to image test patterns on a mask designed to reveal these subtle effects. An example of these experiments is shown in Fig. 10. The key to this test is that the diffraction orders of periodic mask patterns effectively probe different angular regions of the pupil. Therefore, bringing together both small and large features enables us to observe telecentricity differences, side-by-side. In Fig. 10a, notice the through-focus symmetry of the vertical lines, and the narrow depth of focus (DOF) of the fine features. By contrast, in Fig. 10b, observe the asymmetry that occurs on the upper and lower edges of the large feature, and the increased DOF of the fine features, with reduced contrast. These behaviors are consistent with the asymmetric attenuation of vertically diffracted orders arising from the angular response of the multilayer coating. Closer inspection reveals relative position differences between the large and small features through focus.[36]

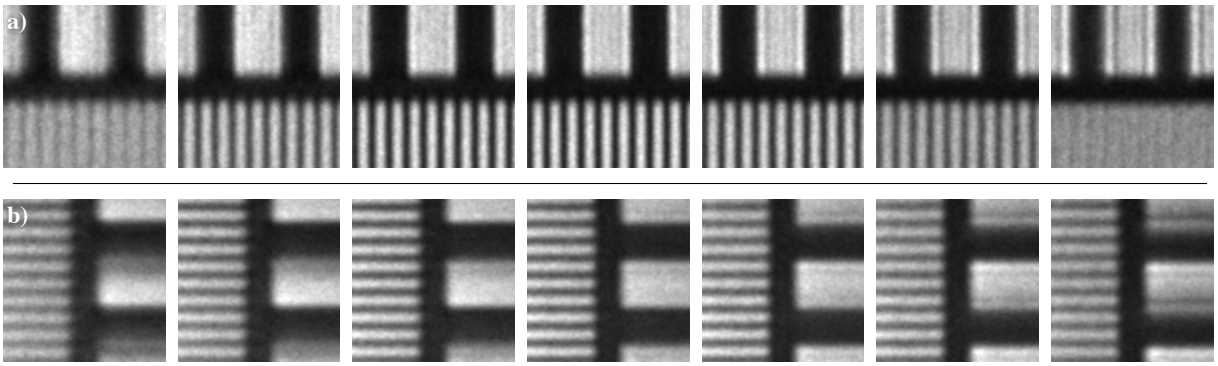

Figure 10. Two through-focus image series with **(a)** vertical and **(b)** horizontal 1:1 lines, imaged with 0.35 4xNA lens and 400 nm focal steps. The image details are 1.5-μm wide, and the smaller lines are 80-nm half-pitch (in mask units). The through-focus and left-right symmetry of the vertical lines is compared to the asymmetry of the horizontal lines. Differences are attributable to a diffraction order imbalance caused by the non-uniform response of the mask with respect to angle.

6. ANAMORPHIC OPTICS

Recently, there has been considerable discussion on the use of *anamorphic optics* as a future path for EUV projection lenses.[37–39] Anamorphic lenses, those with different magnifications in the horizontal and vertical directions, can help to overcome a major hurdle related to the angular reflectivity of the multilayers, discussed in the previous section.

Without significant changes in design, the limited angular response of the multilayer coatings constrains the maximum useful angular range of mask imaging. Furthermore shadowing from the mask absorber topography becomes an increasing concern at larger off-axis angles.[35] These issues are an impediment to any plan to increase the mask-side NA. This includes future projection lens designs with 4× magnification and with higher wafer-side *and* mask-side NA values; or those with higher off-axis central-ray angles (i.e. beyond 6°).

If they can be manufactured to the required tolerances, anamorphic projection optics alleviate this problem by increasing the magnification in the vertical direction only, where the mask-side angles are constrained. The collection solid angle in the horizontal direction (perpendicular to the off-axis plane of incidence) increases on the mask side, in proportion to the the wafer-side NA. Yet, in the vertical direction, parallel to the plane of incidence, the current mask-side angle limitations are maintained, so increasing the *y*-direction magnification allows the wafer-side angles to increase. The resultant pupil can be nearly elliptical in shape (wider in the transverse direction) but remain below a certain, fixed off-axis limit, as shown in Fig. 11. The projection optics would likely be designed to produce a rotationally symmetric, high numerical aperture on the wafer side, possibly at 0.5 or beyond.[38]

SHARP's zoneplate objective lenses can be designed to emulate this elliptical mask-side solid angle without any additional modification to the microscope. SHARP projects images onto the CCD detector with high-magnification; scaling the images to wafer or mask coordinates is performed mathematically with a simple constant length multiplier. To emulate anamorphic lenses, SHARP would continue to project its image onto the CCD in the same manner, but the

mathematical conversion into wafer coordinates would be done with different scaling factors in the horizontal and vertical directions, representing the two anamorphic magnification ratios. In addition, the angular illumination pattern would stretch in a manner that matches the pupil shape.

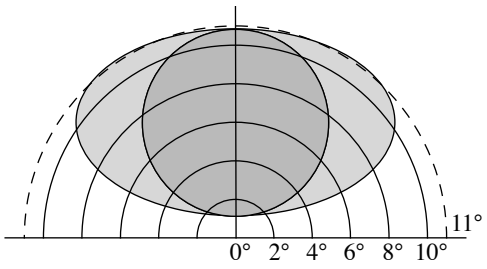

Figure 11. Angular description of the mask-side pupil acceptance angles, with the 0°, normal ray at the bottom center, and each circular arc tracing out constant off-axis angles of incidence. The darker gray circle is centered at 6° central ray angle and represents 0.33 4xNA; it all falls within 11° of normal. The ellipse is an example of what an anamorphic pupil may look like on the mask side. As drawn, the ellipse is stretched horizontally by a factor of 1.7.

7. CONCLUSION

From its inception, SHARP's design considered several possible directions for the future of EUV lithography as it marches toward ever-smaller printed features sizes. The extension and demonstration of SHARP's capabilities in these areas are all subjects of active research. These areas include increased resolution, free-form coherence engineering from illuminator designs, extracting phase from aerial image measurements, investigating high-angle multilayer coating effects, and the extension of SHARP to emulate of anamorphic optics. This broad spectrum of EUV photomask topics covers the major mask- and optics-related advances in our field, and enters the areas where research must move beyond simulation. In addition to its work emulating contemporary EUVL tools, SHARP is ready to continue its role, making additional contributions to current and future topics of high interest and great importance.

8. ACKNOWLEDGMENT

This work was funded by SEMATECH, and performed by University of California Lawrence Berkeley National Laboratory under the auspices of the U.S. Department of Energy, Contract No. DE-AC02-05CH11231. The authors are grateful for the support of SEMATECH project manager Anne Rudack. We appreciate John Managa's and *Intel's* generous assistance in the creation of the Calibration Test Mask. The authors are indebted to Chris Anderson, Patrick Naulleau, the team of the BMET, and *Inpria* for their support in creating the Wafer Test Mask. We also thank Ryan Miyakawa (LBNL), Yow-Gwo Wang and Rene Claus (UC Berkeley) for many interesting discussions about phase measurement modes. QUASAR™ is a trademark of ASML, Netherlands.

REFERENCES

[1] K. A. Goldberg, I. Mochi, S. B. Rekawa, N. S. Smith, *et al.*, "An EUV Fresnel zoneplate mask-imaging microscope for lithography generations reaching 8 nm," *Proc. SPIE* **7969**, 79691O (2011).

[2] K. A. Goldberg, I. Mochi, M. P. Benk, C. Lin, *et al.*, "The SEMATECH high-NA actinic reticle review project (SHARP) EUV mask-imaging microscope ," *Proc. SPIE* **8880**, 88800T (2013).

[3] K. A. Goldberg, I. Mochi, M. Benk, A. P. Allezy, *et al.*, "Commissioning an EUV mask microscope for lithography generations reaching 8 nm," *Proc. SPIE* **8679**, 867919 (2013).

[4] K. A. Goldberg, M. P. Benk, A. Wojdyla, I. Mochi, *et al.*, "Actinic mask imaging: Recent results and future directions from the SHARP EUV Microscope," *Proc. SPIE* **9048**, 90480Y (2014).

[5] P. Naulleau, K. A. Goldberg, P. Batson, P. Denham, *et al.*, "A synchrotron-based Fourier-synthesis custom-coherence illuminator," *AIP Conf. Proc.* **705**, 792–5 (2004).

[6] M. P. Benk, R. H. Miyakawa, W. Chao, Y.-G. Wang, *et al.*, "Broader view on extreme ultraviolet masks: adding complementary imaging modes to the SHARP microscope," *J. Micro/Nanolith. MEMS MOEMS* **14** (1), 013507 (2015).

[7] Y.-G. Wang, R. Miyakawa, W. Chao, K. Goldberg, *et al.*, "Phase-enhanced defect sensitivity for EUV mask inspection," *Proc. SPIE* **9235**, 92350L (2014).
[8] Y.-G. Wang, R. Miyakawa, A. Neureuther, P. Naulleau, "Zernike Phase Contrast Microscope for EUV mask inspection," *Proc. SPIE* **9048**, 904810 (2014).
[9] M. Lawliss, E. Gallagher, M. Hibbs, K. Seki, *et al.*, "Repairing native defects on EUV mask blanks," *Proc. SPIE* **9235**, 923516 (2014).
[10] E. Gallagher, A. Wagner, M. Lawliss, G. McIntyre, *et al.*, "Learning from native defects on EUV mask blanks," *Proc. SPIE* **9256**, 92560K (2014).
[11] Y.-G. Wang, R. Miyakawa, W. Chao, M. P. Benk, *et al.*, "Enhancing Defect Detection with Zernike Phase Contrast in EUV Multilayer Blank Inspection," *Proc. SPIE* **9422**, (2015) *to be published*.
[12] T. Isogawa, K. Seki, M. Lawliss, E. Gallagher, *et al.,* "Screening EUV mask absorbers for defect repair," *Proc. SPIE* **9256**, 92560N (2014).
[13] G. R. McIntyre, E. E. Gallagher, T. E. Robinson, A. C. Smith, "Through-focus EUV multilayer defect repair with nanomachining," *Proc. SPIE* **8679**, 86791I (2013).
[14] P.-Y. Yan, G. Zhang, E. M. Gullikson, K. A. Goldberg, *et al.*, "Understanding EUV mask blank surface roughness induced LER and associated roughness requirement," *Proc. SPIE* **9422**, (2015) *to be published*.
[15] M. Burkhardt, "Best focus shift for thick masks," *Proc. SPIE* **9422**, (2015), *to be published.*
[16] M. P. Benk, D. G. Johnson, A. Donoghue, A. Wojdyla, K. A. Goldberg, "Source optimization at the SHARP microscope," International Symposium on Extreme Ultraviolet Lithography, October 27, 2014, Washington D.C.
[17] P. Naulleau, K. A. Goldberg, E. H. Anderson, K. Bradley, *et al.*, "Status of EUV micro-exposure capabilities at the ALS using the 0.3-NA MET optic," *Proc. SPIE* **5374**, 881–91 (2004).
[18] A. Grenville, "Metal Oxide Photoresists: the Path from Lab to Fab," 2014 International Symposium on Extreme Ultraviolet Lithography, Washington D.C., October 27, 2014.
[19] H. Meiling, W. de Boeij, F. Bornebroek, N. Harned, *et al.* "From performance validation to volume introduction of ASML's NXE platform," *Proc. SPIE* **8322**, 83221G (2012).
[20] J. Bekaert, B. Laenens, S. Verhaegen, L. Van Look, *et al.* "Freeform illumination sources: An experimental study of source-mask optimization for 22 nm SRAM cells," *Proc. SPIE* **7640**, 764008 (2010).
[21] R. Socha, X. Shi, D. LeHoty, "Simultaneous source mask optimization (SMO)," *Proc. SPIE* **5853**, 180–93 (2005).
[22] S. Hsu, L. Chen, Z. Li, S. Park, "An innovative Source-Mask co-Optimization (SMO) method for extending low k1 imaging," *Proc. SPIE* **7140**, 714010 (2008).
[23] X. Liu, R. Howell, S. Hsu, K. Yang, *et al.* "EUV source-mask optimization for 7nm node and beyond," *Proc. SPIE* **9048**, 90480Q (2014).
[24] M. P. Benk, D. G. Johnson, A. Donoghue, A. Wojdyla, "Source optimization at the SHARP microscope," 2014 International Symposium on Extreme Ultraviolet Lithography, Washington D.C., October 27, 2014.
[25] I. Mochi, K. A. Goldberg, R. Xie, P.-Y. Yan, "Quantitative evaluation of mask phase defects from through-focus EUV aerial images," *Proc. SPIE* **7969**, 79691X (2011).
[26] I. Mochi, K. A. Goldberg, S. Huh, "Actinic imaging and evaluation of phase structures on EUV lithography masks," *J. Vac. Sci. Technol. B* **28** (6), C6E11-16 (2010).
[27] S. B. Mehta, C. J. R. Sheppard, "Quantitative phase-gradient imaging at high resolution with asymmetric illumination-based differential phase contrast," *Opt. Lett.* **34** (13), 1924–26 (2009).
[28] L. Tian, J. Wang, L. Waller, "3D differential phase-contrast microscopy with computational illumination using an LED array," *Opt. Lett.* **39** (5), 1326–9 (2014).
[29] C. Krautschik, M. Ito, I. Nishlyama, K. Otaki, "Impact of the EUV mask phase response on the asymmetry of Bossung curves as predicted by rigorous EUV mask simulations," *Proc. SPIE* **4343**, 392–401 (2001).
[30] P.-Y. Yan, "Understanding Bossung curve asymmetry and focus shift effect in EUV lithography," *Proc. SPIE* **4562**, 279–287 (2002).
[31] G. Zheng, R. Horstmeyer, C. Yang, "Wide-field, high-resolution Fourier ptychographic microscopy," *Nat. Photonics* **7**, 739–745 (2013).
[32] L. Tian, X. Li, K. Ramchandran, L. Waller, "Multiplexed coded illumination for Fourier Ptychography with an LED array microscope," *Biomed. Opt. Exp.*, **5** (7), 2376–89 (2014).
[33] A. Wojdyla, M. P. Benk, D. G. Johnson, A. Donoghue, "Fourier Ptychography Microscopy with the SHARP EUV Microscope for increased imaging resolution based on illumination diversity," 2014 International Symposium on Extreme Ultraviolet Lithography, Washington D.C., October 27, 2014.

[34] V. Philipsen, E. Hendrickx, E. Verduijn, S. Raghunathan, "Imaging impact of multilayer tuning in EUV masks, experimental validation," *Proc. SPIE* **9235**, 92350J (2014).
[35] J. Ruoff, "Impact of mask topography and multilayer stack on high NA imaging of EUV masks," *Proc. SPIE* **7823**, 78231N (2010).
[36] S. Raghunathan, O. R. Wood II, P. Mangat, E. Verduijn, *et al.* "Experimental measurements of telecentricity errors in high-numerical-aperture extreme ultraviolet mask images," *J. Vac. Sci. Technol. B* **32** (6), 06F801 (2014).
[37] S. Migura, B. Kneer, J. T. Neumann, W. Kaiser, *et al.*, "EUV Lithography Optics for sub 9 nm Resolution," 2014 International Symposium on Extreme Ultraviolet Lithography, Washington D.C., October 29, 2014.
[38] J. B. P. van Schoot, K. van Ingen Schenau, S. Migura, "EUV lithography scanner for sub-8nm resolution," *Proc. SPIE* **9422**, (2015) *to be published*.
[39] B. Kneer, S. Migura, J. T. Neumann, W. Kaiser, *et al.* "EUV lithography optics for sub-9nm resolution," *Proc. SPIE* **9422**, (2015) *to be published*.